

Edge-Propagation Discharge Mechanism in CF_x Batteries – a First Principles and Experimental Study

Kevin Leung,^{1*} Noah B. Schorr,¹ Matthew Mayer,² Timothy
N. Lambert,¹ Y. Shirley Meng,² and Katharine L. Harrison¹

¹*Sandia National Laboratories, Albuquerque,
NM 87185, United States*

kleung@sandia.gov

²*NanoEngineering,
University of California at San Diego*

(Dated: July 6, 2021)

Abstract

Graphite fluoride (CF_x) cathodes coupled with lithium anodes yield one of the highest theoretical specific capacities (>860 mAh/g) among primary batteries. In practice, the observed discharge voltage (~ 2.5 V) is significantly lower than thermodynamic limits (>4.5 V), the discharge rate is low, and so far Li/CF_x has only been used in primary batteries. Understanding the discharge mechanism at atomic length scales will improve practical CF_x energy density, rate capability, and rechargeability. So far, purely experimental techniques have not identified the correct discharge mechanism or explained the discharge voltage. We apply Density Functional Theory calculations to demonstrate that a CF_x -edge propagation discharge mechanism based on lithium insertion at the CF/C boundary in partially discharged CF_x exhibits a voltage range of 2.5 to 2.9 V — depending on whether solvent molecules are involved. The voltages and solvent dependence agrees with our discharge and galvanostatic intermittent titration technique measurements. The predicted discharge kinetics are consistent with CF_x operations. Finally, we predict Li/CF_x rechargeability under the application of high potentials, along a charging pathway different from that of discharge. Our work represents a general, quasi-kinetic framework to understand the discharge of conversion cathodes, circumventing the widely used phase diagram approach which most likely does not apply to Li/CF_x because equilibrium conditions are not attained in this system.

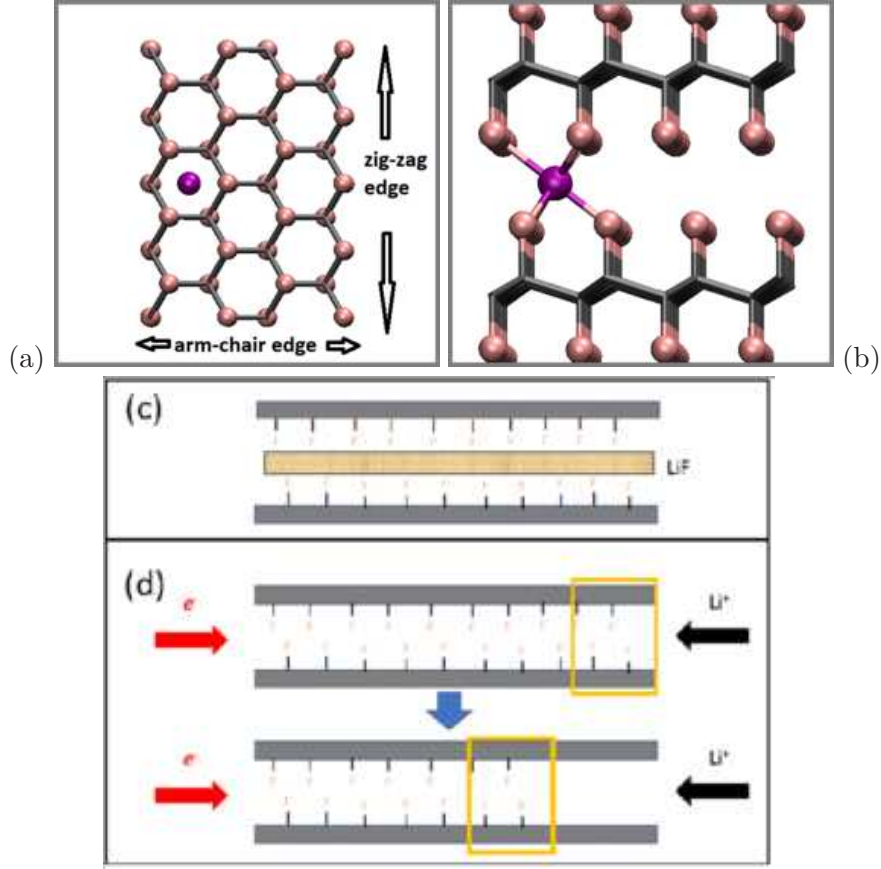
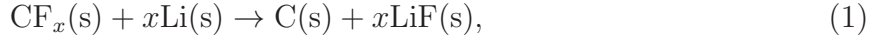


FIG. 1: (a)-(b) Two views of CF_x sheets at $x=1$; zig-zag and arm-chair edges (in analogy with graphite) are indicated. A Li-atom is hypothetically inserted between two CF_x sheets. C, F, and Li atoms are depicted as grey, pink, and purple spheres or sticks. (c)-(d) Schematics of LiF intermediate phase and edge-propagation CF_x discharge mechanism, respectively. Yellow lines highlight local active discharge regions. Black sticks are C-F bonds.

I. INTRODUCTION

Graphite fluoride has the chemical formula CF_x with $0 < x \leq (1 + \delta)$. When fully fluorinated ($x \sim 1$), CF_x cathodes exhibit one of the highest theoretical specific capacities (864 mAh/g) among cathode materials,¹ and have been commercialized as primary lithium battery cells.^{2,3} CF_x is typically synthesized by enforcing chemical reactions between F_2 gas and graphite or other forms of conductive carbon at elevated temperatures.⁴⁻⁷ Idealized models of $x=1$ samples have layers of CF with each carbon atom chemically bonded to three other C and one F atoms (Fig. 1a-b). The registry between adjacent sheets has been predicted to have minimal effect on the total energy.⁸

Li/CF_x batteries discharge via the overall reaction



where “(s)” denotes the solid state. Using thermodynamic data and Eq. 1, the average theoretical voltage is estimated at 4.57 V at $x=1$; it is even higher at smaller x , reaching 5.07 V at $x=0.7$.¹ In practice, the usable energy density is significantly lower than expected from thermodynamics. Li/CF_x batteries discharge at a plateau voltage of $<\sim 2.5$ V at rates of 0.05 C or less (Fig. 2a,c,d). The observed voltage variation is a small fraction of a volt when using different carbon precursor materials,⁹ or electrolytes — including both organic solvents,^{10,11} solid electrolytes,¹² and liquified gas electrolytes (Fig. 2d).^{13,14} Galvanostatic intermittent titration technique (GITT) measurements, which should circumvent most kinetic limitations, have reported CF_x discharge voltages below 3.1 V (Fig. 2b).¹⁵ CF_x materials with more “ionic” C-F bonds, synthesized at x values substantially lower than unity, are reported to yield slightly higher voltage plateaus and higher discharge rates at the expense of lower overall capacities.^{16–18} Disordered/nanoscale carbon precursors also yield rate capability improvement.^{19,20} Unlike Li/CF_x, Na/CF_x batteries have been demonstrated to be rechargeable.^{21–24}

Achieving performance near the ideal theoretical values as predicted by thermodynamics will significantly broaden the application space and impact of CF_x batteries. A detailed elucidation of the CF_x discharge mechanism at the atomic length-scale is required in order to ultimately achieve increased voltage windows, higher energy densities, higher power capability, and improved rechargeability. Several discharge mechanisms have been proposed to explain the voltage profiles; they differ by whether intermediate phases, edge planes, and/or solvent molecules are involved.

Mechanism A: Two Phase Behavior In the absence of intermediate phases, the discharge should exhibit two-phase behavior, and the observed voltage should follow Eq. 1.^{25,26} The reason for the discrepancy between the thermodynamic (>4.57 V) and observed (~ 2.5 V) discharge voltages is then ascribed to slow kinetics and/or nanosize effects associated with LiF/NaF products. One argument against such a two-phase behavior is that Eq. 1 predicts an increase of the equilibrium voltage \mathcal{V}_i as discharge proceeds (x decreases),¹ which has not been observed (Fig. 2).

Mechanism B: Intermediate Phase Alternatively, an intermediate phase has been invoked

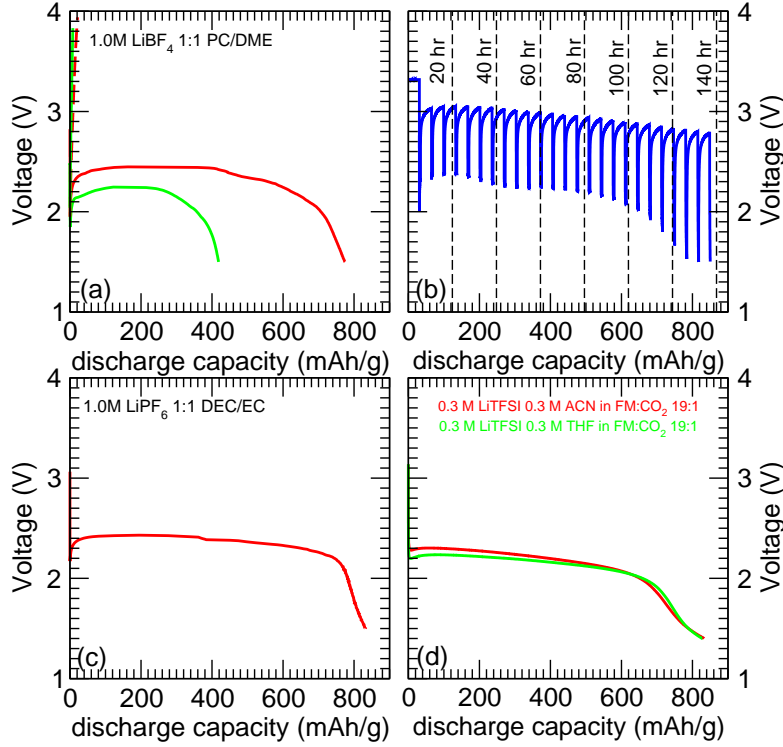
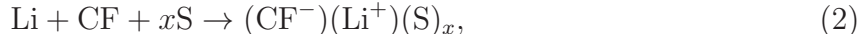


FIG. 2: (a) Galvanostatic discharge and charge of CF cells with PC/DME/Li⁺/BF₄⁻ electrolyte. Cells were left at open circuit voltage for 20 hrs then cycled at a rate of C/20 (red) or C/5 (green). Plot shows that faster rate results in a lower discharge capacity and that neither cell shows any electrochemical reversibility (attempted recharge in dashed lines); CF_{1.09} is the initial composition. (b) GITT of a cell with the same build as those in panel (a) CF cell using a 1.789 mA current pulse, corresponding to a discharge rate of C/20, with a 30 min pulse time and 5 hr rest. The final capacity of the GITT measurement is 825.90 mAh/g. (c) Galvanostatic discharge profile with DEC/EC/Li⁺/PF₆⁻ electrolyte. (d) Galvanostatic discharge of CF cells with two liquified gas electrolytes (LGE) at C/20 rate; CF_{1.05} is the initial composition.

to explain the 2.5 V plateau. This may be a ternary phase such as CLi_xF,²⁷ which can be a thin sheet of one or more LiF layers intercalated between CF_x or C sheets (Fig. 1c).^{24,27} In this case, Eq. 1 does not govern the discharge voltage. Changing CF_x lattice constants with discharge have been reported in *in situ* X-ray analysis,^{28,29} which may suggest such a LiF intercalation structure. However, Mechanism (B) appears less consistent with CF_x not in stack-like configurations, e.g., those synthesized using carbon nanotube precursors.

Mechanism C: Edge-Mediated Another candidate for the intermediate phase is a solvent-coordinated Li^+ complex,^{3,30}



where “S” is a solvent molecule. Such a mechanism necessarily requires an edge-propagation rather than bulk-phase reaction pathway. Edge-propagation mechanisms are attractive because they would be consistent with an extended plateau voltage region independent of the extent of the state-of-charge (x). This is because if the discharge behavior only depends on the local configuration (Fig. 1d), to a first approximation the spatial location of discharge, dependent on x , would not affect the discharge voltage. This is consistent with the appearance of a near constant voltage discharge plateau (Fig. 2a). However, the intermediate phase associated with this mechanism would be small and hard to detect via X-ray diffraction.^{28,29}

Mechanisms (B) and (C) are not mutually exclusive. Strictly speaking, Mechanism (B) does not completely specify a discharge pathway, in terms of the order in which C-F bonds are broken. If thermodynamic equilibrium is assumed, i.e., C-F bonds are broken in ascending order of bond energies, Mechanism (B) may be consistent with an overall, lower average discharge voltage than 4.57 V, but would fail to explain why the observed discharge voltage does not increase with decreasing x (Fig. 2), like thermodynamics would predict.¹ However, when combined with Mechanism (C), the formation of a CLi_xF phase (Fig. 1c) may follow edge-mediated C-F bond-breaking events.

So far, purely experimental efforts have not definitively determined the mechanism. Computational work will shed light on Mechanisms (A)-(C). Regarding Mechanism (A), two-phase-like solid state conversion reactions are well understood and routinely modeled using a phase-diagram approach.^{31,32} The effect of nanosized charge/discharge products has been addressed within the framework of phase diagram calculations to explain the discrepancy between bulk phase thermodynamics predictions and observed battery discharge profiles.^{24,33} However, nanosizing is usually insignificant for particle size on the order of 10 nm, which have been reported as the dimensions of LiF discharge products,²⁶ although further experimental work is needed to ascertain the size distribution. Furthermore, the phase diagram approach assumes equilibrium conditions and reversible reactions. While this is true of many conversion cathode materials,^{31,32} rechargeability associated with Eq. 1 has yet to be demonstrated in any electrolyte, which suggests that equilibrium conditions do not apply.

In the SI (Sec. S2), we further report that Density Functional Theory (DFT) electronic structure calculations predict a barrier for the exchange of two neighboring F-vacancies on a CF sheet that is far too large to permit diffusion, consistent with previous bond-strength calculations.^{34,35} This shows that different C-F bond configurations in CF_x materials are not at equilibration with each other.

Regarding Mechanisms (B) and (C): in this work, we apply DFT to show that Mechanism (C), even without solvent molecules, gives good agreement with experiments. Motivated by edge-initiated discharge in graphite used as lithium ion battery anodes,^{36–38} we examine edge-propagation CF_x discharge (Fig. 1d). We find that Li or Na intercalation into interfacial sites between insulating CF and conductive, defluorinated graphite regions constitutes a small “intermediate phase” most consistent with the observed CF_x discharge voltage plateau (Fig. 2). This intermediate dovetails with classic “interfacial charge storage” behavior.^{39,40} Li insertion is followed by defluorination at the CF/C interface and then further Li insertion, leading to quasi-one-dimensional, row-by-row defluorination and subsequent formation of LiF. LiF formation energetics does not determine the voltage. In addition to CF_x stacks, our model is applicable to CF_x flakes and fluorinated carbon nanotubes with small curvatures, as long as their discharge involves row-by-row defluorination. In this work, we adopt idealized, defect free, partially defluorinated CF_x with zig-zag and arm-chair edges. Defects in carbon sheets and other heterogeneity (e.g., C-F vs. C-F₂ distributions^{41–43}) also affect CF_x battery operations; these complexities will be deferred to future modeling work.

Our calculations also consider Li/ CF_x recharge and discharge rates. Regarding solvent effects: given the large variation in the binding energies between Li^+ and different solvent molecules we will discuss, the solvent dependence of discharge voltage reported in the literature, on the order of 0.2 V, appears surprisingly small and requires further elucidation.^{30,44} This will be addressed by adding solvent molecules at CF_x edge sites in DFT simulations, and comparing to our measurements done in two solvents. A significant amount of DFT modeling work on CF_x have been reported.^{8,35,45–54} Few of them deal with CF_x edges; however, this prior research provides significant guidance and starting structures for the work discussed below.

system	dimensions	stoichiometry	k -sampling	Figure
zig-zag	$6.10 \times 2.60 \times 32.00$	$\text{C}_{18}\text{F}_{20}$	$3 \times 10 \times 1$	
zig-zag	$6.10 \times 5.21 \times 32.00$	$\text{C}_{36}\text{F}_{40}$	$3 \times 5 \times 1$	
zig-zag	$6.10 \times 7.81 \times 32.00$	$\text{C}_{54}\text{F}_{60}$	$3 \times 3 \times 1$	
arm-chair	$6.10 \times 4.63 \times 32.00$	$\text{C}_{36}\text{F}_{40}$	$3 \times 6 \times 1$	
arm-chair	$6.10 \times 9.65 \times 32.00$	$_{72}\text{F}_{80}$	$3 \times 3 \times 1$	
zig-zag/ Li^+	$12.20 \times 10.40 \times 32.00$	$\text{C}_{144}\text{F}_{128}\text{Li}$	$2 \times 5 \times 1$	Fig. 3a
zig-zag/ Li^+	$12.20 \times 10.40 \times 32.00$	$\text{C}_{144}\text{F}_{80}\text{Li}$	$2 \times 5 \times 1$	Fig. 3f
zig-zag/ Li^+	$12.20 \times 20.80 \times 32.00$	$\text{C}_{288}\text{F}_{256}\text{Li}$	$2 \times 5 \times 1$	
arm-chair/ Li^+	$12.20 \times 9.27 \times 36.00$	$\text{C}_{144}\text{F}_{112}\text{Li}$	$2 \times 3 \times 1$	Fig. 6a
arm-chair/ Li^+	$12.20 \times 9.27 \times 44.00$	$\text{Au}_{40}\text{C}_{144}\text{F}_{112}\text{Li}$	$2 \times 3 \times 1$	Fig. 6b
zig-zag/ Li^+	$12.20 \times 10.40 \times 44.00$	$\text{C}_{144}\text{F}_{200}\text{Li}_{72}$	$2 \times 5 \times 1$	Fig. 7a

TABLE 1: Computational details of representative simulation cells. The dimensions are in units of \AA^3 .

II. METHOD

To calculate energies associated with voltages (Eq. 1-2), we apply static DFT calculations with periodically replicated simulation cells, the Vienna Atomic Simulation Package (VASP) version 5.3,^{55–58} and the Perdew-Burke-Ernzerhof (PBE) functional.⁵⁹ A 400 eV planewave energy cutoff is imposed, except that a 500 eV cutoff is used when optimizing simulation cell sizes. We adopt a 6.1 \AA CF_x inter-sheet spacing, similar to Ref. 8.

Our DFT simulation cells represent stacked, partially defluorinated CF_x sheets with sharp interfaces between the fully defluorinated graphene and fully fluorinated (CF) regions. The simulation cell sizes correspond to CF, not graphite, lattice constants; hence strain develops in the defluorinated region.⁴⁶ Representative simulation cell dimensions, stoichiometries, and Brillouin zone sampling settings are listed in Table 1. Other calculations involve variations on these cells. All simulation cells considered are overall charge-neutral. The dipole moment correction is applied in all but a few calculations which do not contain a vacuum region.⁶⁰ This correction only avoids charge/image-charge interactions in the z direction perpendicular to the CF/C interface. When the simulation cell exhibits significant dipole moments, systematic increase of cell size in the lateral directions is still necessary to converge relevant

energy differences. Spin-polarized DFT is used except for certain arm-chair edge calculations with even number of electrons, where non-spin-polarized DFT gives the same result. A few calculations apply the generally more accurate DFT/HSE06 functional.^{61–63} The dispersion-corrected optB86b-vdW functional is also tested in some cases.⁶⁴ The electronic voltage is determined using the work function approach, which is possible in the absence of liquid electrolytes.⁶⁵

We also perform finite temperature *ab initio* molecular dynamics (AIMD) simulations of a small Li cluster in contact with zig-zag or arm-chair edges. These are short-circuit condition simulations which help motivate the sharp CF/C boundaries used in T=0 K DFT simulation cells. A Nose thermostat imposes T=350 K conditions. The simulations adopt Γ -point Brillouin zone sampling; other settings are the same as those discussed above. The zig-zag edge AIMD cell has a $17.93 \times 13.01 \times 28 \text{ \AA}^3$ dimension and a $\text{C}_{150}\text{F}_{180}\text{Li}_{21}$ stoichiometry. The arm-chair edge simulation cell has a $18.30 \times 13.51 \times 28 \text{ \AA}^3$ dimension and a $\text{C}_{126}\text{F}_{144}\text{Li}_{21}$ stoichiometry. The results are described in the SI.

Experimental details are discussed in the SI.

III. RESULTS

A. Experimental Results

Discharge and GITT profiles for CF_x cells with propylene carbonate (PC)/1,2-dimethoxyethane (DME)/lithium tetrafluoroborate (LiBF_4) electrolytes are depicted in Fig. 2a-b. They are similar to results reported in the literature for Li/ CF_x batteries.^{66,67} Fig. 2a shows that the discharge voltage profile exhibits a plateau around 2.4 V at the C/20 rate; discharge voltage and capacity become much more limited at the faster C/5 rate. Recharging does not occur at either rate when an upper voltage cut-off of 4.0 V is imposed. The GITT results (Fig. 2b) show that the highest observed discharge voltage after the initial pulse is ~ 3.05 V. The instantaneous diffusion constants associated with Fig. 2b are depicted in the SI (Fig. S1). Omitting the first two pulses, we estimate that the average Li^+ diffusion constant to be $4.47 \times 10^{-12} \text{ cm}^2/\text{s}$ assuming Li^+ enters the cathode via an ion-insertion pathway (not just a surface reaction). This value is two to three orders of magnitude slower than in commercial secondary lithium-ion battery materials, but does not appear forbid-

dingly slow.⁶⁸ The galvanostatic discharge profile of an electrolyte with ethylene carbonate (EC)/diethyl carbonate (DEC)/lithium hexafluorophosphate (LiPF₆) (Fig. 2c) is similar to that without EC (Fig. 2a).

Galvanostatic discharge data of two fluoromethane (FM)-based liquified gas electrolytes (LGE), with lithium bis(trisfluoromethanesulfonyl)imide (LiTFSI) salt, CO₂ additive, and either 0.3 M acetonitrile (ACN) or 0.3 M tetrahydrofuran (THF), show lower discharge voltages compared with carbonate-based liquid electrolyte at the same C/20 rate (Fig. 2d). This solvent variation will be compared with DFT studies below.

B. Intrinsic Defluorination Thermodynamics Does not Explain Voltage

The equilibrium voltage \mathcal{V}_i associated with a small defluorination increment δx along a particular defluorination pathway,



is given by

$$|e|\mathcal{V}_i = -[E(\text{CF}_x) - E(\text{CF}_{x-\delta x})]/\delta x + E(\text{LiF}) - E(\text{Li}), \quad (4)$$

where the energies $E()$ all refer to those of solid phases. The larger a C-F bond energy ($[E(\text{CF}_x) - E(\text{CF}_{x-\delta x})]/\delta x$) for a particular carbon atom, the lower is the voltage required to defluorinate that atom. Note that more positive \mathcal{V}_i and more negative energy changes mean more favorable reactions with Li. We stress that \mathcal{V}_i can only be realized in experiments if the corresponding reaction step occurs under equilibrium conditions.

First we discuss the energetics of bulk phase CF_x defluorination without metal content in the simulation cell. In this formulation, the effect of Li^+ is solely manifested in the LiF formation energy (Eq. 4). Similar calculations have been applied in previous DFT studies of CF_x batteries.^{8,45–53} No CF_x edge or solvent molecule is included in this approach. Using the PBE, HSE06, and optB86b-vdW functionals, the equilibrium voltages associated with Eq. 1 at $x=1$ (i.e., averaging the voltage defluorinating the entire CF material) are found to be $\mathcal{V}_i=4.38, 4.40$, and 5.16 V, respectively. Periodically replicated CF_x or graphene sheets instead of 3-dimensional structures for both “CF” and “C” in Eq. 1 yield similar results, except that the optB86b-vdW functional voltage is slightly lowered to 5.11 V. The

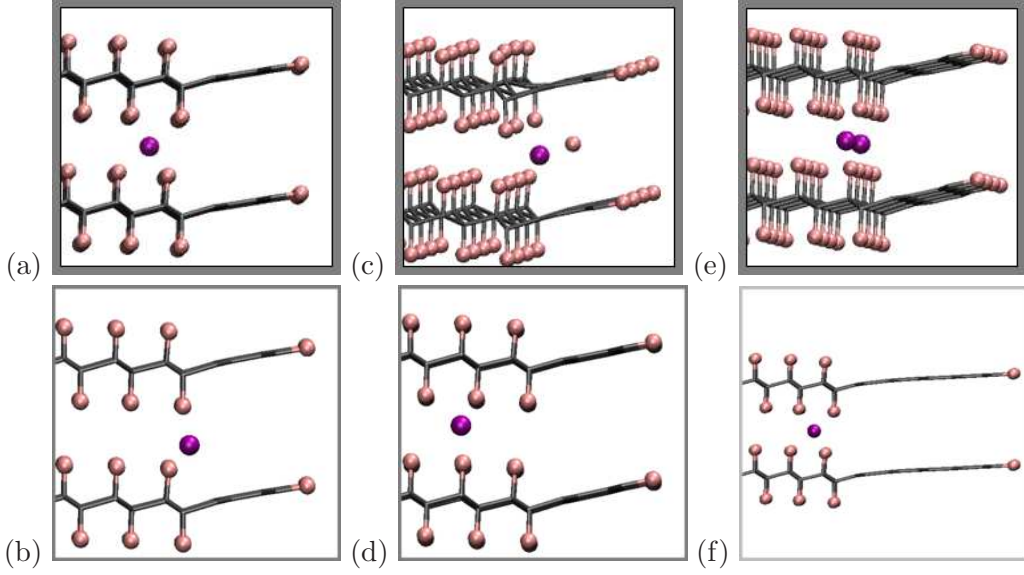


FIG. 3: (a) 6-coordinated CF/C Li “interfacial site.” (b) 3-coordinated Li “outer binding site.” (c) Breaking a C-F bond in panel (b). (d) 6-coordinate Li-site inside the CF/C interface. (e) Inserting two Li at nearby CF/C interfacial sites. (f) CF/C interface site after further removal of several rows of F atoms from panel (a). For color key, see Fig. 1.

PBE and HSE06 functionals are in closest agreement with thermodynamic data,¹ and the computationally less costly PBE is applied for the remainder of this work.

We also consider starting at the $x \rightarrow 1$ limit and removing two neighboring F atoms from a periodically replicated CF sheet via Eq. 5. A $\text{C}_{48}\text{F}_{48}$ model is used (i.e., $\delta x = 1/24$, defluorinating a small portion of the CF). Eq. 3 coupled with Eq. 4 yields $\mathcal{V}_i = 2.86$ V, which is significantly lower than the average value of 4.38 V. See Table 2. This PBE-predicted trend, whereby \mathcal{V}_i increases with state of discharge (smaller x), is qualitatively consistent with thermodynamic data,¹ but is inconsistent with observed electrochemical discharge voltage profiles (Fig. 2). We have not considered intermediate values of x partly because of the multiplicity of possible defluorination configurations with complex energy landscapes,⁴⁶ and partly because our edge-propagation mechanism described below provides a more physical, quasi-kinetic pathway for the sequence of F-atom to be removed, than a global optimal energy criterion.

system	\mathcal{V}_i	figure	notes
bulk CF_x	4.38 V	NA	averaged over $x < 1$
bulk CF_x	2.86 V	NA	at $x=1$ only
bulk $\text{CF}_x + \text{Li}$	0.93 V	Fig. 1a-b	insert Li
zig-zag	2.62 V	Fig. 3a	insert Li
zig-zag	1.45 V	Fig. 3e	insert 2nd Li
zig-zag	2.56 V	Fig. 3f	further defluorination
zig-zag	2.90 V	Fig. 5a	with EC
zig-zag	2.49 V	Fig. 5b	with FM
zig-zag	2.66 V	Fig. 5d	sheet, with EC
zig-zag	2.25 V	Fig. 5f	sheet, with FM
arm-chair	1.49 V	Fig. 6a	insert Li
arm-chair	1.81 V	Fig. 6b	with Au(111)

TABLE 2: Computed voltages (\mathcal{V}_i) at different configurations. Bulk defluorination voltages follow Eq. 1 or 4 while Li-insertion voltages follow Eq. 5. EC and FM are ethylene carbonate and fluoromethane, respectively.

C. Li-insertion Energetics at Zig-Zag CF/C Interface

During CF_x discharge, Li^+ should be present at the CF_x edge facing the electrolyte (right side of Fig. 1d). Simultaneously, an e^- is injected from the current collector (not explicitly included in our DFT model) on the left side. The added e^- moves infinitely fast in ground state DFT calculations; therefore operationally these two charge injection steps are consistent with adding a Li atom on the surface facing the electrolyte. In the SI (Sec. S7), we describe *ab initio* molecular dynamics simulations of Li nanoclusters in contact with and reacting with CF_x edges under short-circuit conditions. These are qualitative in nature, aimed to illustrate what can spontaneously occur under artificially accelerated conditions.

In this section we consider inserting one Li at a time, which is more relevant to slow discharge rate conditions seen in practical CF_x cells. Fig. 3a depicts such a Li at the zig-zag edge interface between CF and the defluorinated graphite region of partially defluorinated CF_x . The existence of sharp CF/C boundaries is motivated by our hypothesis that an edge-

propagation mechanism would not significantly depend F Li-content (x in CF_x , Fig. 1d), and to a lesser extent by AIMD simulation results (SI). At this “CF/C interfacial site,” Li is coordinated to six C-F groups.

Unlike the formation of LiF discharge products, which involves typically slower nucleation events, Li^+ insertion into CF_x is diffusive, assisted by electric fields. It should be fast (Sec. III A)³⁰ and reversible. This equilibrium assumption allows the use of

$$|e|\mathcal{V}_i = [E(\text{CFLi}_x) - E(\text{CFLi}_{x-\delta x})]/\delta x - E(\text{Li}), \quad (5)$$

to describe the observed voltage. Eq. 5 would be identical to expressions used to calculate LiC_6 equilibrium voltages if “CF” is replaced with “C.” In this formulation, LiF(s) formation subsequent to Li insertion does not figure into \mathcal{V}_i , unlike in most previous DFT work. We find that Li insertion at the interfacial site (Fig. 3a) yields $\mathcal{V}_i=2.62$ V via Eq. 4. This value is in good agreement with the observed CF_x discharge plateau value of ~ 2.5 V (Fig. 1a). GITT measurements, which should give voltages closer to equilibrium values, yield open circuit voltage values higher by only 0.4-0.5 V. This covers the \mathcal{V}_i range predicted.

This value of 2.62 V is surprising in light of the less favorable Li insertion into bulk CF, both fluorinated and defluorinated. Li^+ intercalation into graphite (as model for defluorinated CF_x) has been extensively studied in the context of graphite anodes. The process is fast and reversible, even though an electron-insulating but ion-conducting solid electrolyte interphase film is present.^{38,71} This reaction,



occurs at $\mathcal{V}_i=0.1\text{-}0.2$ V vs. $\text{Li}^+/\text{Li(s)}$, which is far lower than the observed CF_x discharge voltages (Fig. 2). In contrast, the equilibrium voltages associated with Li-insertion into CF_x stacks (Fig. 1a),



have not been reported. Our DFT/PBE calculations in the dilute limit ($x=1/48$) yield 0.93 V vs. $\text{Li}^+/\text{Li(s)}$. This \mathcal{V}_i is higher than that associated with LiC_6 , but is significantly lower than experimental discharge voltages (Fig. 2). Since the excess e^- from Li insertion will reside in the conduction band of the insulating CF, the 0.93 V value is likely overestimated because the PBE functional underestimates band gaps. This value is consistent with the

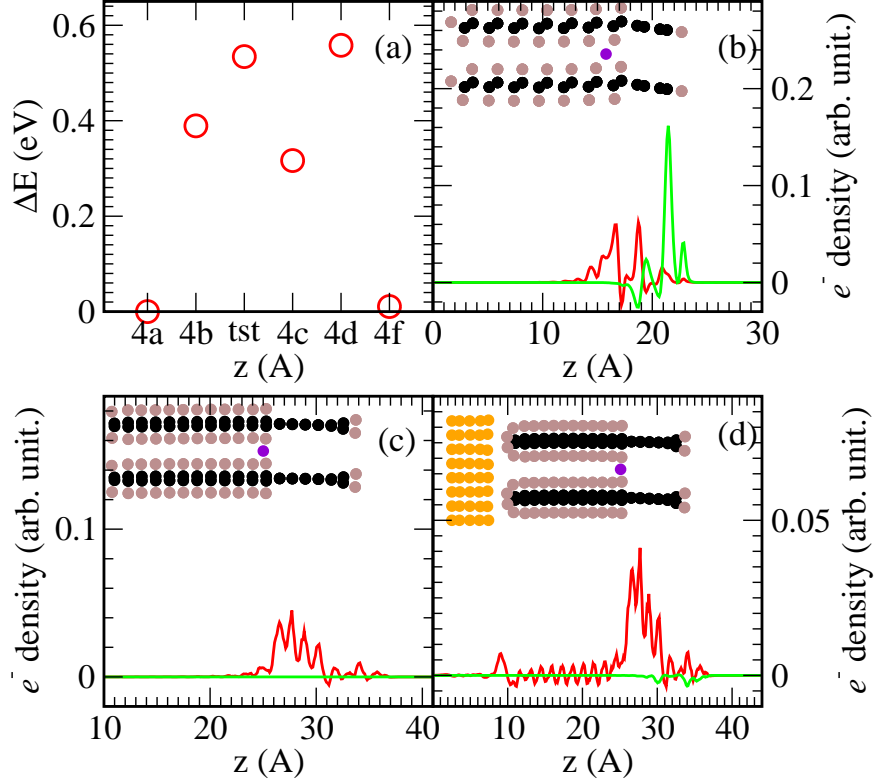


FIG. 4: (a) Energy landscape for Fig. 3 [recall panel (f) refers to a different F-content]. (b)-(d) Differential charge (red) and spin (green) densities before/after removing a Li atom. (b) Zig-zag edge; the Li is at $z=15.8$ Å. (c) Arm-chair CF/C interfaces; the Li is at $z=15.2$ Å. (d) Same as (c) but with an Au(111) slab on the left side; Li is at $z=25.2$ Å. For color key, see Fig. 1.

defect-free single CF sheet voltage of ~ 1.0 V reported in Ref. 54 after adjusting the Li atom binding energy used therein with the lithium metal cohesive energy reference.

The anomalously high \mathcal{V}_i at the interface compared to bulk phases is a manifestation of interfacial charge storage behavior.^{39,40} Li^+ favors insertion into the CF region, where it is stabilized by CF polar groups, while the accompanying e^- is partially delocalized in the nearby metallic carbon region. This charge sharing principle is illustrated in the differential charge and spin density plot (Fig. 4b), computed by removing the inserted Li atom while freezing all other atoms. In contrast, while graphite is metallic and readily accommodates an excess e^- , it interacts weakly with Li^+ , resulting in a low overall Li-binding energy and a low \mathcal{V}_i . For CF, the interaction between Li^+ and the polar C-F bond is more energetically favorable than that between Li^+ and graphite. However, CF_x is an insulator at large x ,

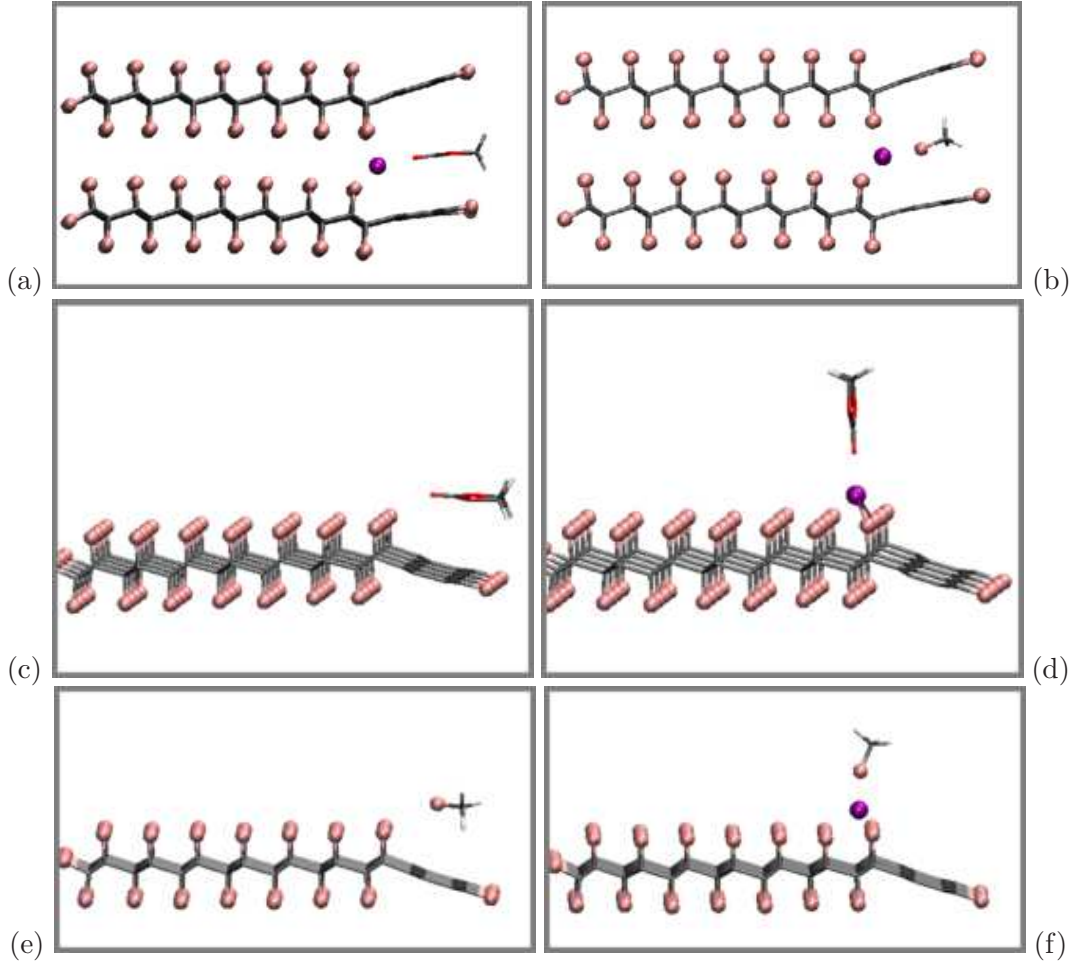


FIG. 5: (a)-(b): Adding a single EC or FM solvent molecule to Li^+ at the 3-coordinated outer binding site at the zig-zag edge. (c): EC on isolated partially defluorinated CF_x sheet. (d): Same as (c) but with Li^+ coordinated to 3 CF bonds and the EC molecule. (e): FM on isolated partially defluorinated CF_x sheet. (f): Same as (e) but with Li^+ coordinated to 3 CF bonds and the FM molecule. \mathcal{V}_i associated with panels (a), (b), (d), and (f) are 2.90 V, 2.49 V, 2.66 V, and 2.25 V, respectively. The color key is as in Fig. 1; in addition red and white sticks represent O and H atoms.

and adding e^- to its conduction band is unfavorable. Hence the interface between CF and defluorinated CF regions is uniquely suited to inserting Li.

D. Subsequent C-F Bond-Breaking Kinetics

Next we consider the steps subsequent to Li insertion. We move the inserted Li to a 3-coordinated surface site outside the interfacial site and re-optimize the configuration (Fig. 3b). This will be referred to as the “outer binding site.” The energy associated with this site is a modest 0.39 eV higher than the interfacial site (Fig. 3a). The subsequent C-F bond breaking event (Fig. 3c), a prerequisite to LiF crystal formation, is exothermic by 0.07 eV relative to Fig. 3b. It is endothermic relative to Fig. 3a by 0.32 eV, but that enthalpy cost is compensated by the canonical ~ 0.4 eV entropy gained by releasing a “molecule” (LiF) at $T=300$ K, due to the transformation of low-entropy vibrational degrees of freedom in a configuration with an intact C-F bond to the high-entropy rotational and translational degrees of freedom after the bond is broken.⁷² The value of ~ 0.4 eV assumes that the system is at equilibrium and the product is at a 1.0 M concentration in the liquid phase. In reality, the LiF product is continuously consumed and removed from the electrolyte, so 0.4 eV is a lower-bound rough estimate (SI Sec. S6). The activation energy (ΔE^*) associated with this defluorination step is a modest 0.53 eV relative to Fig. 3a. Assuming a standard kinetic prefactor of 10^{12} /s, once Li is inserted, F^- will be released in millisecond time scales at $T=300$ K.

Over time, the released LiF diatomic fragment is expected to nucleate with other LiF units to form LiF nanocrystalline discharge products. Experimentally, crystallites of sizes as small as 30 nm have been inferred. These crystallites have been observed to be >10 nm in size,²⁶ bulk like for the purpose of calculating energetics, though more rigorous experimentation is needed to conclusively determine the final LiF dimensions in discharged CF_x cathodes. Our DFT/PBE calculations show that $\text{LiF(g)} \rightarrow \text{LiF(s)}$, where “(g)” and “(s)” stands for gas and crystalline solid phases respectively, is exothermic by 2.66 eV. Therefore LiF nanocrystal formation is not reversible unless >2.66 eV external energy is injected, for example, via applying a high potential (Sec. III G). This may help explain why Li/CF_x cells have so far been non-rechargeable. We have not considered the kinetics or possible overpotentials associated with the subsequent nucleation or growth of LiF crystals from these 2-atom LiF units. However, a reactive molecular dynamics (MD) approach has previously shown that such growth can occur in MD time scales ($\ll 1$ second), in a different battery system.⁷³

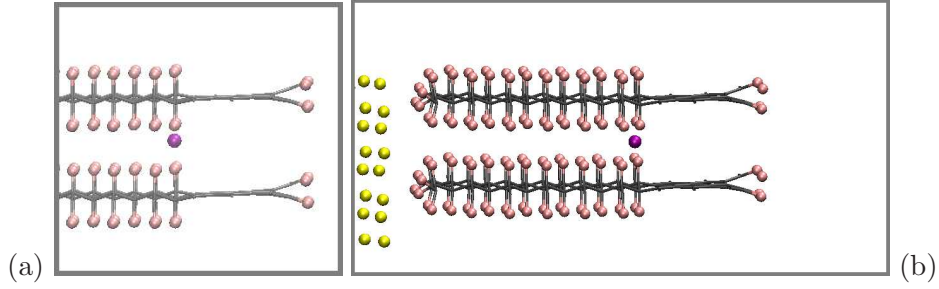


FIG. 6: (a)-(b) Li-insertion at arm-chair edge CF/C interfaces, with and without an Au current collector (yellow).

E. Detailed Analysis of Li Insertion, Solvent Effects

Fig. 3d depicts Li insertion further inside the CF region, away from the interface. It is unfavorable in energy by 0.56 eV relative to the interfacial site (Fig. 3a), likely due to larger charge separation between the Li^+ and the partially delocalized injected e^- . Thus interior CF sites would not be occupied by Li unless the discharge occurs at significant overpotentials. Thus our proposed interfacial discharge intermediate phase is small in length scale and may be difficult to detect experimentally. The F-removal energy landscape with this zig-zag edge is depicted in Fig. 4a. Far from the interface, Li insertion into CF should revert to the $\mathcal{V}_i=0.93$ V reported in Sec. III C.

Fig. 3e depicts adding a second Li atom at an interfacial site near the first. The energy gain in this step corresponds to $\mathcal{V}_i=1.45$ V, which is significantly less favorable than the 2.62 V associated with the first Li. This finding suggests that the interfacial site is not saturated with Li. However, doubling the simulation cell y -dimension (Table 2, lines 6-7, not shown in figures) is found to reduce \mathcal{V}_i by only 0.01 V, suggesting that separation by ~ 1 nm is the saturation limit for interfacial Li atoms.

After removing one F-atom from Fig. 3a, the next discharge event associated with the next Li insertion is 2.72 V (not shown), slightly higher than the 2.62 V before removing that F-atom. The C-F bond cleavage subsequent to this second Li-insertion is also energetically more favorable than before (-0.27 eV compared with +0.32 eV) and the activation energy is lower (+0.32 eV compared with 0.53 eV). The more favorable defluorination energetics is partly a manifestation of an “odd-even” electron spin effect discussed in the SI (Sec. S3). Finally, we consider Li insertion at the interfacial site after a more substantial defluorination.

Removing several rows of F atoms to leave another clean-cut CF/C boundary (Fig. 3f) yields Li intercalation $\mathcal{V}_i=2.56$ V at the interfacial site, which is only slightly less than the 2.62 V associated with Fig. 3a. This conforms with the Fig. 1d hypothesis that the defluorination voltage depends on the local environment, not the global F-content in CF_x . If the F-removal leaves a jagged boundary between the CF and C regions (not shown), \mathcal{V}_i is slightly increased, to 3.12-3.15 V depending on the defluorination extent. We note that row-by-row C-F bond breaking during discharge is limited by the “gatekeeper” site with the lowest local \mathcal{V}_i , which is in the 2.56-2.62 V range. At or below such voltages, a new intact row of CF groups can be defluorinated.

So far we have not addressed solvent effects. Fig. 5a-b depict the addition of a single ethylene carbonate (EC) or fluoromethane (FM) solvent molecule to the Li at the 3-coordinated outer binding site (Fig. 3b); they dovetail with Eq. 2 proposed in the literature.³⁰ EC is a standard battery electrolyte solvent molecule, similar in structure to PC used in Fig. 2a-b; the discharge profile using EC (Fig. 2c) is similar to that without EC. FM (featured in Fig. 2d) is a key component of a recently proposed liquefied gas electrolyte particularly useful at low temperatures.^{13,14} In Fig. 2, PC-based and EC-based electrolytes are found to exhibit discharge plateaus higher in voltage than FM-based electrolyte by 0.1-0.3 V. Our DFT predictions are that \mathcal{V}_i is higher for EC than FM, by 2.90 V vs. 2.49 V (Fig. 3a-b). This difference is only slightly higher than the experimental difference, but is significantly less than the relative gas phase binding energy; we find that an EC binds to a single Li^+ more favorably than FM to Li^+ , by 1.09 V eV. Fig. 5c-f deal with isolated CF_x sheets rather than stacks. They are relevant to the exposed outer basal plane surfaces of CF_x stacks and large curvature, fluorinated nanotubes.²⁴ In these cases, no 6-coordinated Li^+ binding site exists between two CF_x sheets, and solvent molecules may be necessary to stabilize Li adsorption. Here we postulate that isolated CF_x sheets also undergo row-by-row defluorination and exhibit sharp interfaces between CF and C regions. In Fig. 5d, we place a Li at the surface site coordinated to 3 CF bonds and an EC molecule on the zig-zag edge. After optimizing atomic positions, the Li^+ becomes strongly coordinated to two CF groups and less strongly bound to a third CF (Fig. 5d). \mathcal{V}_i for this configuration is 2.66 V, less than the 2.90 V for Fig. 5a but still in reasonable agreement with experimental measurements (Fig. 2). This suggests that our Li^+ intercalation mechanism applies to isolated CF_x sheets, not just stacks. The corresponding value for FM (Fig. 5f) is 2.25 V, less than the 2.49 V for

Fig. 5b.

The \mathcal{V}_i variation due to EC or FM coordination is 0.41-0.42 V, qualitatively similar to those found in our experimental measurements (Fig. 2), further supporting our computational interpretation of CF_x discharge behavior. These \mathcal{V}_i are also within a few tenths of a volt of the solvent-free 2.62 V at the 6-coordinated interfacial site at this F-content (Fig. 3a); they remain far closer to experimental discharge voltages than previous DFT calculations.

We caution that these equilibrium voltages are calculated using a gas phase solvent molecule reference. They ignore solvent-solvent attractive free energies which may add 0.3-0.5 eV to the cost of each solvent molecule. It is difficult to estimate the EC or FM desolvation free energy contribution because the electrolytes have mixed solvents and salts, the DFT/PBE method underestimates dispersion forces between solvent molecules and between solvent molecules and graphite sheets, and the entropy contributions involved are difficult to estimate. However, in the Fig. 5d,f configurations, if a liquid solvent were in the simulation cell, the EC or FM coordinated to Li^+ would have been partially surrounded by solvent molecules. So these configurations would exhibit far less desolvation corrections than Fig. 5a-b, where embedding EC and FM between graphite sheets would hinder them from interacting with other solvent molecules. Despite this difference, the $\Delta\mathcal{V}_i$ predicted when using EC (Fig. 5d) and FM (Fig. 5f) molecules is almost the same as that associated with Fig. 5a-b. This strongly suggests that bulk liquid effects do not strongly modify our conclusion about solvent differences predicted in vacuum.

We stress that the true \mathcal{V}_i in any electrolyte is bounded from below by the solvent-free value. If solvent-coordinated Li^+ at the outer binding site is not more favorable than the solvent-free interfacial site (Fig. 3a), the solvent will not contribute to \mathcal{V}_i . This helps explain the limited electrolyte-dependence observed during Li/CF_x discharge (Fig. 2 and Refs. 10–12), compared to the much larger dependence of gas phase binding energies on solvent molecules. Note also that we choose the solvent models here to compare with our measurements. In the future, we will consider solvents found in commercial Li/CF_x cells like γ -butyrolactone.⁷⁴

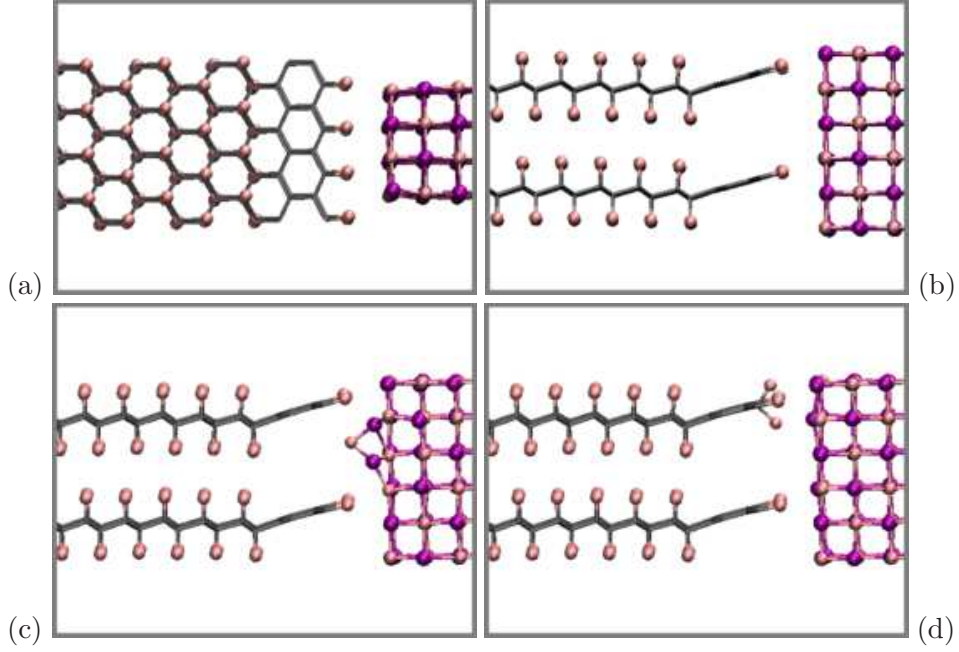


FIG. 7: (a)-(b) Two views of the finite LiF slab at zig-zag surface of CF/C interface; (c) F^- moved to inner surface; (d) formation of C-F bond. LiF is three bilayer ($\sim 12 \text{ \AA}$) thick in the z direction (left-to-right).

F. Arm-Chair Edges

As discussed in the SI (Sec. S4), arm-chair edge CF_x partially defluorinated in the direction normal to the edge yields insulating carbon because of tensile strain. If the periodic boundary condition is removed in the lateral direction so the model represents a finite sheet, this carbon will likely spontaneously develop a curvature, reducing the strain and the electronic band gap. However, the CF_x/C interface region may still exhibit local strain, which may be measurable in Raman spectroscopy.^{75,76} In this work, we focus on periodically replicated arm-chair edges.

Fig. 6a depicts the insertion of a Li atom into the arm-chair interfacial site, which is coordinated to 4 C-F groups. In this configuration, \mathcal{V}_i is 1.49 V, lower than the zig-zag edge value. This is consistent with the fact that it now costs extra energy to deposit an e^- into the conduction band of the system because of the finite band gap (SI Sec. S4). Charge density changes induced by Li-insertion (Fig. 4c) show that the excess e^- still causes somewhat localized changes at the interface, but over a larger graphite region than zig-zag.

In a working battery cathode, metallic electrode behavior is maintained by adding con-

ductive carbon additives and depositing the material on to a current conductor. CF_x is also converted to conductive carbon upon discharge. In Fig. 6b, we add a Au(100) current collector to the system to qualitatively mimic a electronically conducting component. \mathcal{V}_i is predicted to be 1.81 V, which is 0.32 V more favorable than the model without Au (Fig. 6a) but is still significantly lower than the zig-zag value of 2.62 V, or experimental discharge voltages (Fig. 2). Therefore an external current collector does not strongly alter the equilibrium voltage associated with Li insertion. The excess density plot (Fig. 4d) shows significant delocalization of excess e^- over the CF region, but little of the excess charge is on the Au electrode, likely because the metallic region is too far from the interface to yield benefits. We conclude that CF/C interfaces at zig-zag edges are more active than those at arm-chair edges in terms of CF_x discharge. In the SI (Sec. S5), we consider electronic voltage effects in this system.⁶⁵

We have also examined the outer binding site with Li^+ coordinated to 3 C-F bonds and an EC molecule (not shown but analogous to Fig. 5a). \mathcal{V}_i is 1.96 V in this case, substantially lower than either measurement with carbonate electrolytes (Fig. 2a,c) or the 2.92 V zig-zag edge value. These calculations demonstrate the importance of a metallic carbon region in CF_x discharge.

In the SI, we also compare insertion of Na rather than Li into CF_x (Sec. S8). The predicted voltages are found to be similar but the C-F bond-breaking event exhibits a larger barrier and is slower. We speculate that multiple Na^+ coordinated to one C-F group may reduce the C-F bond-breaking barrier there and play a role in Na/ CF_x discharge.

G. Recharge Calculations

In this section, we return to the Li/ CF_x zig-zag edge model (Fig. 3a) and consider Li/ CF_x recharge. We add a LiF slab outside the partially defluorinated CF_x edge (Fig. 7a, Table 1). The slab is periodically replicated in the direction perpendicular to the CF_x sheets, but is finite in extent in the other lateral direction (Fig. 7a-b). This baseline model system mimics discharged LiF residing on the defluorinated CF_x edge.

Next, a F^- anion is moved from the outer LiF surface to its inner surface closest to the CF_x edge, where it is now coordinated to two Li^+ ions (Fig. 7c). This configuration mimics voltage-driven F^- diffusion through the LiF discharge product towards the defluo-

minated carbon, where it ultimately reconstitutes a C-F bond. The energy cost associated with creating the defect (Fig. 7c) from the defect-free sheet (Fig. 7a-b) is 2.44 eV in this $12.2 \times 10.4 \times 44.0 \text{ \AA}^3$ simulation cell. This periodically replicated cell is charge neutral, but exhibits a significant dipole moment which can lead to electrostatic energy artifacts.⁷⁸ Using larger, $1 \times 2 \times 1$ and $2 \times 2 \times 1$ surface supercells, the energy costs are $\Delta E = 2.14 \text{ eV}$ and 2.21 eV respectively, suggesting that this energy has converged to within $\sim 0.1 \text{ eV}$. During recharge, this energy cost needs to be provided by changing the applied electronic voltage \mathcal{V}_e .⁶⁵ A more complete discussion of \mathcal{V}_e is given in the SI (Sec. S5). Fig. 7d depicts a configuration where the F^- on the inner LiF surface is further transferred to the carbon region to form a C-F bond. $\Delta E = -0.26 \text{ eV}$ relative to Fig. 7c, and the barrier is a small $\Delta E^* = 0.19 \text{ eV}$. This suggests that reformation of C-F bonds from nearby undercoordinated F^- anions can readily occur; formation of this bond is not the prohibitive rate-limiting step.

To show that a voltage change can cause F^- diffusion from the LiF outer surface to its inner surface prior to C-F bond formation, we create an artificial electric field by removing a Li^+ from the outer interface of the LiF slab. In terms of electronic voltage,⁶⁵ the Li^+ vacancy causes the Fig. 7a-b \mathcal{V}_e to increase from 4.02 V to 6.46 V. This latter \mathcal{V}_e is artificially high, partly because of the lack of a liquid electrolyte beyond the outside surface of the LiF slab. However, \mathcal{V}_e includes contributions from many interfaces, including the LiF/vacuum and C/LiF interfaces which should be similar before and after Li^+ vacancy formation. It is the electric field across the LiF slab, reflected in the voltage difference between the two cases ($\Delta \mathcal{V}_e = +2.44 \text{ V}$), that is relevant to our calculation.

Upon creating the Li^+ vacancy on the outer LiF surface, the Fig. 7c configuration is no longer metastable, unlike the case without the Li^+ vacancy. The ΔE for moving a F^- from the outer LiF surface (Fig. 7d) to the inner surface and reforming a C-F bond decreases from an endothermic $+2.19 \text{ eV}$ to an exothermic (favorable) -0.93 eV in the $1 \times 1 \times 1$ surface cell. The corresponding ΔE for the $2 \times 2 \times 1$ surface cell is even more favorable at -1.45 eV . These ΔE 's strongly suggest that refluorination, and recharging, are energetically and kinetically viable near the outer defluorinated CF_x surface in contact with LiF discharge products if a sufficient electric field is applied.

Note that we have focused on reforming a C-F bond at the outer defluorinated CF_x surface, not the CF/C interface which is the focus of the discharge calculations (Fig. 3). Therefore we assume recharge occurs “from outside in.” The reason is that we assume F^-

anions are poorly solvated by organic solvent molecules. This suggests that moving F^- to the CF/C interface may entail a large barrier. (In contrast, Li^+ is much better solvated by organic solvents and can be readily transported to the CF/C interface via $Li^+(\text{solvent molecule})_n$ complexes and can initiate discharge there.) If this hypothesis is correct, CF_x charge and discharge will follow different pathways. This may be an important consideration when designing practical rechargeable Li/ CF_x cathodes.

IV. CONCLUSIONS

The existence of a CF_x discharge “intermediate phase” has been proposed in the literature to explain the discharge behavior of Li/ CF_x batteries, but its identity has so far not been elucidated. In this work, we hypothesize an intermediate phase associated with a CF_x edge-propagation Li-insertion mechanism. Our DFT calculations show that Li intercalation at the zig-zag edge boundary between fluorinated (i.e., CF) and defluorinated (carbon) regions exhibits an equilibrium voltage about 2.6 V vs. $Li^+/Li(s)$. The predicted voltage range is in good agreement with experimental CF_x electrochemical discharge voltage profiles, and is only 0.4-0.5 V lower than GITT measurements. Li-insertion is favorable there because of partial separation of Li^+ and e^- charges at the interface, in accordance with “interfacial charge storage” paradigm.³⁹ Na/ CF_x is predicted to exhibit similar discharge voltages (SI). Our proposed CF_x intermediate phase has a spatial extent limited to the CF/C interface thickness. These predictions should assist renewed experimental attempt to locate the CF_x intermediate phase. Our predicted voltages do not involve C-F bond breaking or LiF nucleation energetics.

This proposed mechanism is not inconsistent with the existence of a thin, several-atom-thick LiF layer that may reside between CF_x sheets, swelling the cathode material in the process. Indeed, our hypothesis may provide a viable pathway to realize a $CF_x:Li_y$ intermediate phase. We also show that post Li-insertion CF_x discharge kinetics, especially C-F bond breaking, are sufficiently fast in Li/ CF_x batteries when a C-F bond is polarized by the inserted Li^+ cation nearby. The proposed discharge mechanism helps explain why solvent dependence on discharge voltage should be small. Our predicted variation in voltage plateau values as the electrolyte varies is in qualitative agreement with our discharge measurements in organic carbonate and liquified gas electrolytes. Finally, we propose that Li/ CF_x recharge

may proceed via a pathway distinct from the one encountered during discharge.

Our computational work does not invoke phase diagram calculations, and therefore does not assume that CF_x and LiF are in equilibrium. Since Li/CF_x batteries are not rechargeable so far, the equilibrium assumption appears untenable. Thus our work provides a novel, general framework for understanding and modeling the discharge behavior of new types of primary batteries. For example, in recent work on SF_6 -based primary batteries, the equilibrium assumption underlying traditional phase diagram approach also seems inapplicable.⁷⁷ For future work, electric field and electronic voltage effects need to be addressed more explicitly by including liquid electrolytes in more rigorous AIMD simulations. CF_x heterogeneity^{41–43} will also be considered to further improve our discharge voltage predictions.

Supporting Information for Publication

Supporting information is available free of charge on the ACS Publications website at DOI:xxx: experimental details; F-vacancy diffusion barriers in CF_x ; odd-even energetic effects on defluorination; local electronic densities of state; electronic voltage discussions; entropy considerations; short-circuit AIMD simulations; Na/CF_x predictions.

Acknowledgement

We thank Brennan Walder, Todd Alam, Jessica Rimsza, and Hayley Hirsh for useful input and discussions. This project was supported by Sandia Laboratory Directed Research and Development (LDRD) project 218253. Sandia National Laboratories is a multi-mission laboratory managed and operated by National Technology and Engineering Solutions of Sandia, LLC., a wholly owned subsidiary of Honeywell International, Inc., for the U.S. Department of Energy’s National Nuclear Security Administration under contract DE-NA-0003525. This paper describes objective technical results and analysis. Any subjective views or opinions that might be expressed in the paper do not necessarily represent the views of the U.S. Department of Energy or the United States Government.

References

- ¹ Wood, J.L. *et al.* Thermodynamic, Electrochemical and Synthetic Studies of the Graphite-Fluorine Compounds CF and C₄F. *National Technical Information Service* **1972**, AD-755 934.
- ² Zhang, Q.; Takeuchi, K.J.; Takeuchi, E.S.; Marschilok, A.C. Progress Towards High-Power Li/CF_x Batteries: Electrode Architectures using Carbon Nanotubes with CF_x. *Phys. Chem. Chem. Phys.* **2015**, *17*, 22504-22518.
- ³ Amatucci, G.G.; Pereira, N. Fluoride Based Electrode Materials for Advanced Energy Storage Devices. *J. Fluorine Chem.* **2007**, *128*, 243-262.
- ⁴ Watanabe, N. Two Types of Graphite Fluorides, (CF)_n and (C₂F)_n, and Discharge Characteristics and Mechanisms of Electrodes of (CF)_n and (C₂F)_n, in Lithium Batteries. *Solid State Ionics* **1980**, *1*, 87-110.
- ⁵ Hagiwara, R.; Nakajima, T.; Watanabe, N. Kinetic Study of Discharge Reaction of Lithium-Graphite Fluoride Cell. *J. Electrochem. Soc.* **1988**, *135*, 2128-2133.
- ⁶ Yazami, R.; Hamwi, A. A New Graphite Fluoride Compound as Electrode Material for Lithium Intercalation in Solid State Cells. *Solid State Ionics* **1988**, *28-30*, 1756-1761.
- ⁷ Zhong, G.; Chen, H.; Cheng, Y.; Meng, L.; Liu, H.; Liu, Z.; Zheng, G.; Xiang, Y.; Liu, X.; Li, Q.; Zhang, Q.; Yue, H.; Lu, C.; Yang, Y. Insights into the Lithiation Mechanism of CF_x by a Joint high-Resolution ¹⁹F NMR, *in situ* TEM and ⁷Li NMR Approach. *J. Mater. Chem. A* **2019**, *7*, 19793-19799.
- ⁸ Han, S.S.; Yu, T.H.; Merinov, B.V.; van Duin, A.C.T.; Yazami, R.; Goddard, W.A. Unraveling Structural Models of Graphite Fluorides by Density Functional Theory Calculations. *Chem. Mater.* **2010**, *22*, 2142-2154.
- ⁹ Watanabe, N.; Endo, M.; Ueno, K. Cathodic Discharge of Graphite Fluoride, (CF)_n, Prepared from Several Carbon Materials, in Lithium Organic Electrolyte Batteries. *Solid State Ionics* **1980**, *1*, 501-507.
- ¹⁰ Pang, C.; Ding, F.; Sun, W.; Liu, J.; Hao, M.; Wang, Y.; Liu, X.; Xu, Q. A Novel Dimethyl Sulfoxide/1,3-Dioxolane Based Electrolyte for Lithium/Carbon Fluorides Batteries with a High Discharge Voltage Plateau. *Electrochim. Acta* **2015**, *174*, 230-237.

- ¹¹ Watanabe, N.; Hagiwara, R.; Nakajima, T.; Touhara, H.; Ueno, K. Solvent Effects on Electrochemical Characteristics of Graphite Fluoride-Lithium Batteries. *Electrochem. Acta* **1982**, *27*, 1615-1619.
- ¹² Rangasamy, E.; Li, J.; Sahu, G.; Dudney, N.; Liang, C. Pushing the Theoretical Limit of Li-CF_x Batteries: A Tale of Bifunctional Electrolyte. *J. Am. Chem. Soc.* **2014**, *136*, 6874-6877.
- ¹³ Rustomji, C.S.; Yang, Y.; Kim, T.K.; Mac, J.; Kim, Y.J.; Caldwell, E.; Chung, H.; Meng, Y.S. Liquefied Gas Electrolytes for Electrochemical Energy Storage Devices. *Science* **2017**, *356*, 1351.
- ¹⁴ Yang, Y.; Davies, D.M.; Yin, Y.; Borodin, O.; Lee, J.Z.; Fang, C.; Olguin, M.; Zhang, Y.; Sablina, E.S.; Wang, X.; Rustomji, C.S.; Meng, Y.S. High-Efficiency Lithium-Metal Anode Enabled by Liquefied Gas Electrolytes. *Joule* **2019**, *3*, 1986-2000.
- ¹⁵ Kickol, A.; Schied, T.; Heubner, C.; Schneider, M.; Michaelis, A.; Bobeth, M.; Cuniberti, G. GITT Analysis of Lithium Insertion Cathodes for Determining the Lithium Diffusion Coefficient at Low Temperature: Challenges and Pitfalls. *J. Electrochem. Soc.* **2020**, *167*, 090546.
- ¹⁶ Lam, P.; Yazami, R. Physical Characteristics and Rate Performance of (CF_x)_n (0.33<*x*<0.66) in Lithium Batteries. *J. Power Sources* **2006**, *153*, 354-359.
- ¹⁷ Yoshida, K.; Sugawara, Y.; Saitoh, M.; Matsumoto, K.; Hagiwara R.; Matsuo, Y.; Kuwabara, A.; Ukyo, Y.; Ikuhara, Y. Microscopic Characterization of the C-F Bonds in Fluorine-Graphite Intercalation Compounds. *J. Power Sources* **2020**, *445*, 227320.
- ¹⁸ Gurein, K.; Dubois, M.; Hamwi, A. Electrochemical Discharge Mechanism of Fluorinated Graphite Used as Electrode in Primary Lithium Batteries. *J. Phys. Chem. Solids* **2006**, *67*, 1173-1177.
- ¹⁹ Dai, Y.; Cai, S.; Wu, L.; Yang, W.; Xie, J.; Wen, W.; Zheng, J.-C.; Zhu, Y. Surface Modified CF_x Cathode Material for Ultrafast Discharge and high Energy Density. *J. Mater. Chem. A* **2014**, *2*, 20896-20901.
- ²⁰ Giraudet, J.; Dubois, M.; Inacio, J.; Hamwi, A. Electrochemical Insertion of Lithium Ions into Disordered Carbons Derived from Reduced Graphite Fluoride. *Carbon*, **2003**, *41*, 453-463.
- ²¹ Liu, W.; Li, H.; Xie, J.-Y.; Fu, Z.-W. Rechargeable Room-Temperature CF_x-Sodium Batteries. *ACS. Appl. Mater. Interfaces*, **2014**, *6*, 2209-2212.
- ²² Liu, W.; Shadike, Z.; Liu, Z.-C.; Liu, W.-Y.; Xie, J.-Y.; Fu, Z.-W. Enhanced Electrochemical Activity of Rechargeable Carbon Fluorides-Sodium Battery with Catalysts. *Carbon*, **2005**, *93*,

- 523-532.
- ²³ Liu, W.; Li, Y.; Zan, B.-X.; Shi, B.; Guo, R.; Pei, H.-J.; Xie, J.-Y. Amorphous, Highly Disordered Carbon Fluorides as a Novel Cathode for Sodium Secondary Batteries. *J. Phys. Chem. C*, **2016**, *120*, 25203-25209.
 - ²⁴ Shao, Y.; Yue, H.; Qiao, R.; Hu, J.; Zhong, G.; Wu, S.; McDonald, M.J.; Gong, Z.; Zhu, Z.; Yang, W.; Yong, Y. Synthesis and Reaction Mechanism of Novel Fluorinated Carbon Fiber as a High-Voltage Cathode Material for Rechargeable Na Batteries. *Chem. Mater.* **2016**, *28*, 1026-1033.
 - ²⁵ Zhang, S.S.; Foster, D.; Wolfenstine, J.; Read, J. Electrochemical Characteristic and Discharge Mechanism of a Primary Li/CF_x Cell. *J. Power Sources* **2009**, *187*, 233-237.
 - ²⁶ Read, J.; Collins, E.; Piekarski, B.; Zhang, S. LiF Formation and Cathode Swelling in the Li/CF_x Battery. *J. Electrochem. Soc.* **2011**, *158*, A504-A510.
 - ²⁷ Whittingham, M.S. Mechanism of Reduction of the Fluorographite Cathode. *J. Electrochem. Soc.* **1975**, *122*, 526-527.
 - ²⁸ Nagasubramanian, G.; Rodriguez, M.A. Performance Enhancement at Low Temperatures and In Situ X-ray Analyses of Discharge Reaction of Li/(CF_x)_n Cells. *J. Power Sources* **2007**, *170*, 179-184.
 - ²⁹ Rodriguez, M.A.; Keenan, M.R.; Nagasubramanian, G. *In situ* X-ray Diffraction Analysis of (CF_x)_n Batteries: Signal Extraction by Multivariate Analysis. *J. Appl. Cryst.* **2007**, *40*, 1097-1104.
 - ³⁰ Nakajima, T. Carbon-Fluorine Compounds as Battery Materials. *J. Fluorine Chem.* **1999**, *100*, 57-61.
 - ³¹ Doe, R.E.; Persson, K.; Meng, Y.S.; Ceder, G. First-Principles Investigation of the Li-Fe-F Phase Diagram and Equilibrium and Nonequilibrium Conversion Reactions of Iron Fluorides in Lithium. *Chem. Mater.* **2008**, *20*, 5274-5283.
 - ³² Li, L.; Jacobs, R.; Gao, P.; Gan, L.; Wang, F.; Morgan, D.; Jing, S. Origins of Large Voltage Hysteresis in High Energy-Density Metal Fluoride Lithium-Ion Battery Conversion Electrodes. *J. Am. Chem. Soc.* **2016**, *138*, 2838-2848.
 - ³³ Seo, J.K.; Cho, H.-M.; Takahara, K.; Chapman, K.W.; Borkiewicz, O.J.; Sina, M.; Meng, Y.S. Revisiting the Conversion Reaction Voltage and the Reversibility of the CuF₂ Electrode in Li-ion Batteries. *Nano Research* **2017**, *10*, 4232-4244.

- ³⁴ Dubecky, M.; Otyepkova, E.; Lazar, P.; Karlicky, F., Peter, M.; Cepe, K.; Banas, P.; Zboril, R.; Otyepka, M. Reactivity of Fluorographene: A Facile Way Toward Graphene Derivatives. *J. Phys. Chem. Lett.* **2015**, *6*, 1430-1434.
- ³⁵ Krishnamurthy, V.; Viswanathan, V. Beyond Transition Metal Oxide Cathodes for Electric Aviation: The Case of Rechargeable CF_x . *ACS Energy Lett.* **2020**, *5*, 3330-3335.
- ³⁶ Baba, T.; Sodeyama, K.; Kawamura, Y.; Tateyama, Y. Li-ion Transport at the Interface Between a Graphite Anode and Li_2CO_3 Solid Electrolyte Interphase: *Ab Initio* Molecular Dynamics Study. *Phys. Chem. Chem. Phys.* **2020**, *22*, 10764-10774.
- ³⁷ Leung, K.; Predicting the Voltage Dependence of Interfacial Electrochemical Processes at Lithium-Intercalated Graphite Edge Planes. *Phys. Chem. Chem. Phys.* **2015**, *17*, 1637-1643.
- ³⁸ Cresce, A.v.W.; Borodin, O.; Xu, K. Correlating Li^+ Solvation Sheath Structure with Interphasial Chemistry on Graphite. *J. Phys. Chem. C* **2012**, *116*, 26111-26117.
- ³⁹ Fu, L.; Chen, C.-C.; Samuelis, D.; Maier, J. Thermodynamics of Lithium Storage at Abrupt Junctions: Modeling and Experimental Evidence. *Phys. Rev. Lett.* **2014**, *112*, 208301.
- ⁴⁰ Zhukovskii, Y.F.; Balaya, P.; Dolle, M.; Kotomin, E.A.; Maier, J. Enhanced Lithium Storage and Chemical Diffusion in Metal-LiF Nanocomposites: Experimental and Theoretical Results. *Phys. Rev. B* **76**, 235414 (2007).
- ⁴¹ Krawietz, T.R.; Haw, J.F. Characterization of poly(carbon monofluoride) by ^{19}F and ^{13}C Cross Polarization MAS NMR Spectroscopy. *Chem. Commun.* **1998**, 2151-2152
- ⁴² Cadman, P.; Scott, J.D.; Thomas, J.M. The Fluorination of the Surfaces of Elemental Carbon-I. X-Ray Photoelectron Spectroscopic Studies of Fluorinated Graphite. *Carbon* **1977**, *15*, 75-86.
- ⁴³ Clark, D.T.; Peeling, J. Applications of ESCA to Polymer Chemistry. XII. Structure and Bonding in Commercially Produced Fluorographites. *J. Polymer Sci.* **1976**, *14*, 2941-2967.
- ⁴⁴ Watanabe N.; Hagiwara, R.; Nakajima, T.; Touhara, H.; Ueno, K. Solvents Effects on Electrochemical Characteristics of Graphite Fluoride-Lithium Batteries. *Electrochim. Acta* **1982**, *27*, 1615-1619.
- ⁴⁵ Charlier J.-C.; Gonze, X.; Michenaud, J.-P. First-Principles Study of Graphite Monofluoride $(\text{CF})_n$. *Phys. Rev. B* **1993**, *47*, 16162-16168.
- ⁴⁶ Boukhvalov, D.W. Absence of a Stable Atomic Structure in Fluorinated Graphene. *Phys. Chem. Chem. Phys.* **2016**, *18*, 13287-13293.
- ⁴⁷ Bettinger, H.F.; Kudin, K.N.; Scuseria, G.E. Structural Models of Fluorine-Graphite Intercala-

- tion Compounds from Density Functional Theory. *J. Phys. Chem. A* **2004**, *108*, 3016-3018.
- ⁴⁸ Sahin, H.; Topsakal, M.; Ciraci, S. Structures of Fluorinated Graphene and their Signatures. *Phys. Rev. B* **2011**, *83*, 115432.
- ⁴⁹ Takagi, Y.; Kusakabe, K. Transition from Direct Band Gap to Indirect Band Gap in Fluorinated Carbon. *Phys. Rev. B* **2002**, *65*, 121103.
- ⁵⁰ Karlicky, F.; Zbořil, R.; Otyepka, M. Band Gaps and Structural Properties of Graphene Halides and Their Derivates: A Hybrid Functional Study with Localized Orbital Basis Sets. *J. Chem. Phys.* **2012**, *137*, 034709.
- ⁵¹ Rao, F.; Wang, Z.; Xu, B.; Chen, L.; Ouyang, C. First-Principles Study of Lithium and Sodium Atoms Intercalation in Fluorinated Graphite. *Engineering*, **2015**, *1*, 243-246.
- ⁵² Zhou, S.; Sherpa, S.D.; Hess, D.W.; Bongiorno, A. Chemical Bonding of Partially Fluorinated Graphene. *J. Phys. Chem. C* **2014**, *118*, 26402-26408.
- ⁵³ Shi, H.; Pan, H.; Zhang, Y.-W.; Yakobson, B.I. Electronic and Magnetic Properties of Graphene/Fluorographene Superlattices. *J. Phys. Chem. C* **2012**, *116*, 18278-18283.
- ⁵⁴ Fan, R.; Yang, B.; Ma, D.; Yuan, W.; Ma, J.; Ren, H. First-Principles Study of the Adsorption Behaviors of Li Atoms and LiF on the CF_x ($x=1.0, 0.9, 0.8, 0.5, \sim 0.0$) Surface. *RSC Adv.* **2020**, *10*, 31881-31888.
- ⁵⁵ Kresse, G.; Furthmüller, J. Efficient Iterative Schemes for Ab Initio Total-Energy Calculations Using a Plane-wave Basis Set. *Phys. Rev. B* **1996**, *54*, 11169-11186.
- ⁵⁶ Kresse, G.; Furthmüller, J. Efficiency of *Ab-initio* Total Energy Calculations for Metals and Semiconductors using a Plane-Wave Basis Set. *Comput. Mater. Sci.* **1996**, *6*, 15-50.
- ⁵⁷ Kresse G.; Joubert, D. From Ultrasoft Pseudopotentials to the Projector Augmented-Wave Method. *Phys. Rev. B* **1999**, *59*, 1758-1775.
- ⁵⁸ Paier, J.; Marsman, M.; Kresse, G. Why Does the B3LYP Hybrid Functional Fail for Metals? *J. Chem. Phys.* **2007**, *127*, 024103.
- ⁵⁹ Perdew, J.P., Burke, K.; Ernzerhof, .M. Generalized Gradient Approximation Made Simple. *Phys. Rev. Lett.* **1996**, *77*, 3865-3868.
- ⁶⁰ Neugebauer, J.; Scheffler, M. Adsorbate-Substrate and Adsorbate-Adsorbate Interactions of Na and K adlayers on Al(111). *Phys. Rev. B* **1992**, *46*, 16067-16080.
- ⁶¹ Heyd, J.; Scuseria, G.E.; Ernzerhof, M. Hybrid Functionals based on a Screened Coulomb Potential. *J. Chem. Phys.* **2003**, *118*, 8207-8215.

- ⁶² Heyd, J.; Scuseria, G.E.; Ernzerhof, M. Hybrid Functionals Based on a Screened Coulomb Potential. *J. Chem. Phys.* **2006**, *124*, 219906.
- ⁶³ Vydrov, O.A.; Heyd, J.; Krukau, A.V.; Scuseria, G.E. Importance of Short-Range versus Long-Range Hartree Fock Exchange for the Performance of Hybrid Density Functionals. *J. Chem. Phys.*, **2006**, *125*, 074106.
- ⁶⁴ Klimes, J.; Bowler, D.R.; Michaelides, A. Van der Waals Density Functionals Applied to Solids. *Phys. Rev. B* **2011**, *83*, 195131.
- ⁶⁵ Leung, K. DFT Modelling of Explicit Solid-Solid Interfaces in Batteries: Methods and Challenges. *Phys. Chem. Chem. Phys.* **2020**, *22*, 10412-10425.
- ⁶⁶ Li, Y.; Feng, W. The Tunable Electrochemical Performances of Carbon Fluorides/Manganese Dioxide Hybrid Cathodes by their Arrangements. *J. Power Sources* **2015**, *274*, 1292-1299.
- ⁶⁷ Zhou, P.; Weng, J.; Liu, X.; Li, Y.; Wang, L.; Wu, X.; Zhou, T.; Zhou, J.; Zhuo, S. Urea-Assistant Ball-Milled CF_x as Electrode Material for Primary Lithium Battery with Improved Energy Density and Power Density. *J. Power Sources* **2019**, *414*, 210-217.
- ⁶⁸ Cabanero, M.A.; Boaretto, N.; Röder, M.; Müller, J.; Kallo, J.; Latz, A. Direct Determination of Diffusion Coefficients in Commercial Li-Ion Batteries. *J. Electrochem. Soc.* **2018**, *165*, A847-A885.
- ⁶⁹ Wang, J.; Sun, M.; Liu, Y.; Lin, J.; Wang, L.; Xu, Z.; Wang, W.; Yuan, Z.; Liu, J.; Bai, X. Unraveling Nanoscale Electrochemical Dynamics of Graphite Fluoride by *in situ* Electron Microscopy: Key Difference between Lithiation and Sodiation. *J. Mater. Chem. A* **2020**, *8*, 6105-6111.
- ⁷⁰ Leifer, N.D.; Johnson, V.S.; Ben-Ari, R.; Gan, H.; Lehnes, J.M.; Guo, R.; Lu, W.; Muffoletto, B.C.; Reddy, T.; Stallworth, P.E.; Greenbaum, S.G. Solid-State NMR Studies of Chemically Lithiated CF_x . *J. Electrochem. Soc.* **2010**, *157*, A148-A154.
- ⁷¹ Abe, T.; Fukuda, H.; Iriyama, Y.; Ogumi, Z. Solvated Li-ion Transfer at Interface between Graphite and Electrolyte. *J. Electrochem. Soc.* **2004**, *151*, A1120-A1123.
- ⁷² Leung, K.; Nielsen, I.M.B.; Kurtz, I. *Ab Initio* Molecular Dynamics Study of Carbon Dioxide and Bicarbonate Hydration and the Nucleophilic Attack of Hydroxide on CO_2 . *J. Phys. Chem. B* **2007**, *111*, 4453-4459.
- ⁷³ Ma, Y.; Garofalini, S.H. Atomistic Insights into the Conversion Reaction in Iron Fluoride: A Dynamically Adaptive Force Field Approach. *J. Am. Chem. Soc.* **2012**, *134*, 8205-8211.

- ⁷⁴ Zhang, S.S.; Foster, D.; Read, J. A Low Temperature Electrolyte for Primary Li/CF_x batteries. *J. Power Sources* **2009**, *188*, 532-537.
- ⁷⁵ Hui, J.; Schorr, N.B.; Pakhira, S.; Qu, Z.; Mendoza-Cortes, J.L.; Rodriguez-Lopez, J. Achieving Fast and Efficient K⁺ Intercalation on Ultrathin Graphene Electrodes Modified by a Li⁺ Based Solid-Electrolyte Interphase. *J. Am. Chem. Soc.* **2018**, *140*, 13599-13603.
- ⁷⁶ Sole, C.; Drewett, N.E.; Hardwick, L.J. *In situ* Raman Study of Lithium-Ion Intercalation into Microcrystalline Graphite. *Faraday Discuss.* **2014**, *172*, 223-237.
- ⁷⁷ Li, Y.; Khurram, A.; Gallant, B.M. A High-Capacity Lithium-Gas Battery Based on Sulfur Fluoride Conversion. *J. Phys. Chem. C* **2018**, *122*, 7128-7138.
- ⁷⁸ In simulation cells with large net dipole moments in the *z*-direction and periodically replicated in the *x*- and *y*-directions, the image dipoles repel one another. The energy correction can be estimated by creating a lattice model, provided that the effective dielectric constant is known. See Leung, K.; Criscenti, L.J.; Knight, A.W.; Ilgen, A.G.; Ho, T.; Greathouse, J.A. Concerted Metal Cation Desorption and Proton Transfer on Deprotonated Silica Surfaces. *J. Phys. Chem. Lett.* **2018**, *9*, 5379-5385.

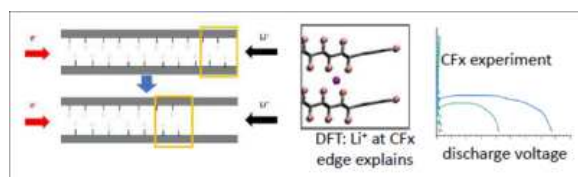


FIG. 8: Table of content Graphic.

